The University of Osaka
Institutional Knowledge Archive

Title	Molecular dynamics analysis of multiphase interfaces based on in situ extraction of the pressure distribution of a liquid droplet on a solid surface
Author(s)	Nishida, S.; Surblys, D.; Yamaguchi, Y. et al.
Citation	The Journal of Chemical Physics. 2014, 140(7), p. 074707
Version Type	VoR
URL	https://hdl.handle.net/11094/82373
rights	This article may be downloaded for personal use only. Any other use requires prior permission of the author and AIP Publishing. This article appeared in The Journal of Chemical Physics 140, 074707 (2014) and may be found at https://doi.org/10.1063/1.4865254.
Note	

Molecular dynamics analysis of multiphase interfaces based on *in situ* extraction of the pressure distribution of a liquid droplet on a solid surface

S. Nishida,[1,a)] D. Surblys,[1,b)] Y. Yamaguchi,[1,c)] K. Kuroda,[2] M. Kagawa,[2] T. Nakajima,[2] and H. Fujimura[2]

[1]*Department of Mechanical Engineering, Osaka University, 2-1 Yamadaoka, Suita 565-0871, Japan*
[2]*R & D Center, Dai Nippon Printing Co., Ltd., 1-1-3 Midorigahara, Tsukuba 300-2646, Japan*

Molecular dynamics simulations of a nanoscale liquid droplet on a solid surface are carried out in order to examine the pressure tensor field around the multiphase interfaces, and to explore the validity of Young's equation. By applying the virial theorem to a hemicylindrical droplet consisting of argon molecules on a solid surface, two-dimensional distribution of the pressure tensor is obtained. Tensile principal pressure tangential to the interface is observed around the liquid-vapor transition layer, while both tensile and compressive principal pressure tangential to the interface exists around the solid-liquid transition layer due to the inhomogeneous density distribution. The two features intermix inside the overlap region between the transition layers at the contact line. The contact angle is evaluated by using a contour line of the maximum principal pressure difference. The interfacial tensions are calculated by using Bakker's equation and Young-Laplace equation to the pressure tensor distribution. The relation between measured contact angle and calculated interfacial tensions turns out to be consistent with Young's equation, which is known as the description of the force balance at the three-phase interface. © *2014 AIP Publishing LLC*. [http://dx.doi.org/10.1063/1.4865254]

I. INTRODUCTION

The behavior of liquid droplet on a solid surface, wetting, is of crucial significance in various science and engineering fields, and the motion of the three-phase interface consisting of liquid, solid, and vapor phases has been widely studied.[1] The contact angle defined as the angle between liquid-vapor and solid-liquid interfaces is commonly used to measure wettability at the macroscopic scale. By introducing the concept of interfacial tensions and contact angle θ, Young's equation[2] is stated as follows:

$$\gamma_{SL} - \gamma_{SV} + \gamma_{LV} \cos \theta = 0, \qquad (1)$$

where γ_{SL}, γ_{SV}, and γ_{LV} denote solid-liquid, solid-vapor, and liquid-vapor interfacial tensions, respectively. This equation describes the horizontal balance of these interfacial tensions at the three-phase interface. Because Eq. (1) was derived for the wetting at the macroscopic scale, various models for the microscopic scale have been put forward, such as introducing microscopic contact angle,[3] adding line tension term to Eq. (1),[4,5] and dealing with precursor films.[6] However, it is difficult to validate these models mainly because experimentally measuring the interfacial tensions containing solid phase is not trivial.[7,8]

Molecular dynamics (MD) simulation is a potent tool for analysis at the microscopic and nanoscopic scale,[9,10] because it is possible to directly observe the independent molecular motion, which has so far been very difficult to do by

experiments, especially for liquids. Nijmeijer *et al.*[11] conducted MD simulations using mono-atomic Lennard-Jones (L-J) fluid film on a solid surface, and demonstrated that the balance indicated by Eq. (1) is applicable there. Ingebrigtsen and Toxvaerd[12] analyzed the droplet shape of L-J nanodroplet in detail, and Weijs *et al.*[13] investigated the origin of line tension for a L-J nonodroplet and its effects on the equilibrium contact angle. Regarding interfacial tensions, Leroy and Müller-Plathe[14] used the phantom-wall method to determine the solid-liquid surface free energy of L-J liquid on smooth and rough surfaces, and Grzelak and Errington[15] applied the grand canonical transition matrix Monte Carlo simulation to compute the interfacial properties. Seveno *et al.*[16] investigated the Young's equation through MD simulations of cylindrical rod dipping into a liquid bath. Surblys *et al.*[17] showed that the balance also holds for droplets consisting of water-alcohol mixture. In these works, the interfacial tensions were evaluated from one-dimensional pressure distributions inside planar liquid film systems which were created separately from the systems used for gauging wettability.

In this study, MD simulations of liquid droplets that are composed of mono-atomic L-J molecules on a solid surface are conducted in order to examine the pressure tensor field around the multiphase interfaces, and also to explore the validity of Young's equation in nanoscale. A quasi-two-dimensional droplet shape is employed to avoid the effect of line tension which is present in three-dimensional spherical droplet with small radius.[12–14] From these droplets, two-dimensional pressure tensor distribution is obtained *in situ* via the virial theorem, and the contact angle and interfacial tensions are calculated by using it. This two-dimensional distribution also provides a new insight about the specific

---
a)Electronic mail: nishida@gcom.mech.eng.osaka-u.ac.jp.
b)Electronic mail: donatas@gcom.mech.eng.osaka-u.ac.jp.
c)Electronic mail: yamaguchi@mech.eng.osaka-u.ac.jp. URL: http://www-gcom.mech.eng.osaka-u.ac.jp/~yamaguchi/.

feature of interfaces especially of the three-phase interface at nanoscopic scale.

II. SIMULATION METHOD

A. Potential model

For ease of physical understanding, argon molecules are adopted as mono-atomic fluid molecules. Concerning interactions between argon molecules, the following 12-6 L-J potential is used:

$$\Phi_{L-J}(r_{ij}) = 4\epsilon_{ij} H(r_c - r_{ij})$$
$$\times \left[\left(\frac{\sigma_{ij}}{r_{ij}}\right)^{12} - \left(\frac{\sigma_{ij}}{r_{ij}}\right)^{6} + c_1 \left(\frac{r_{ij}}{r_c}\right)^{2} - c_2 \right], \quad (2)$$

where r_{ij} is the distance between atoms i and j, while ϵ_{ij} and σ_{ij} denote the L-J energy and length parameters, respectively. This L-J interaction is truncated at a cut-off distance $r_c = 3.5\sigma_{ij}$ using the Heaviside step function H and correction terms are added so that this potential approaches to zero smoothly at r_c with the following coefficients:

$$c_1 = 6 \left(\frac{\sigma_{ij}}{r_c}\right)^{12} - 3 \left(\frac{\sigma_{ij}}{r_c}\right)^{6}, \quad (3)$$

$$c_2 = 7 \left(\frac{\sigma_{ij}}{r_c}\right)^{12} - 4 \left(\frac{\sigma_{ij}}{r_c}\right)^{6}. \quad (4)$$

The solid walls also consist of mono-atomic molecules. A face-centered cubic (FCC) crystal is assumed as the structure of the wall where physical properties of platinum are used for the mass and lattice constants. The inter-atomic potential between wall molecules is expressed by the following harmonic potential connecting the nearest neighbors:

$$\Phi_{\text{harmonic}}(r_{ij}) = \frac{k}{2}(r_{ij} - r_0)^2, \quad (5)$$

where r_0 and k denote the equilibrium distance and spring constant, respectively.

The interactions between argon and wall molecules are also expressed by the L-J potential and the length parameter $\sigma_{\text{Ar-wall}}$ is given by the Lorentz mixing rule:

$$\sigma_{\text{Ar-wall}} = \frac{1}{2}(\sigma_{\text{Ar-Ar}} + \sigma_{\text{wall-wall}}). \quad (6)$$

The energy parameter $\epsilon_{\text{Ar-wall}}$ determines the wettability and is changed as a calculation parameter by multiplying the fluid-solid interaction coefficient η to the base value given by the Berthelot mixing rule:

$$\epsilon_{\text{Ar-wall}} = \eta \sqrt{\epsilon_{\text{Ar-Ar}} \cdot \epsilon_{\text{wall-wall}}}. \quad (7)$$

The value of η is varied so that further comparison to existing studies on similar systems[11–15,18] could be performed. The potential and mass parameters are summarized in Table I.

B. Simulation systems

A system with an argon droplet on a solid surface is simulated in this study. A hemicylindrical shaped droplet with

TABLE I. Potential and mass parameters.

$\sigma_{\text{Ar-Ar}}$ (nm)	$\epsilon_{\text{Ar-Ar}}$ (K)	m_{Ar} (g/mol)	r_0 (nm)	k (N/m)
0.340	121.0	40.0	0.277	46.8
$\sigma_{\text{wall-wall}}$[a] (nm)	$\epsilon_{\text{wall-wall}}$[a] (K)	m_{wall} (g/mol)		
0.350	72.4	195.1		

[a]Used only for Lorentz-Berthelot mixing rule.

a straight contact line achieved by means of the periodic boundary condition is employed in order to avoid the effect of line tension which is not included in Eq. (1),[4] because it has been shown that the contact angle is largely affected by the line tension in a three-dimensional spherical droplet with a large contact line curvature.[13] This hemicylindrical shape also makes it easy to calculate the two-dimensional distribution of the pressure tensor. An FCC (111) surface of a solid crystal with three layers is placed on the bottom of the calculation cell, and the argon droplet is positioned on it. The number densities per area of (111) layer and per volume are $1.74\,\sigma_{\text{Ar-Ar}}^{-2}$ and $2.62\,\sigma_{\text{Ar-Ar}}^{-3}$, respectively, and these values could be used for the further comparison to existing studies on similar systems.[11–15,18] With periodic boundary conditions in lateral x- and y-directions, the droplet is infinity long in the y-direction, while mirror boundary condition is imposed on the top boundary. The calculation region size is $26.0 \times 4.3 \times 12.0$ nm^3, consisting of 4000 argon molecules and 5076 wall molecules. A cylindrical liquid droplet is preliminary equilibrated away from the solid surface, and after its automatic adsorption onto a solid surface through the Brownian motion, an initial equilibrium hemicylindrical droplet there is obtained with a further run of more than 1 ns. The position of wall molecules in the bottom layer is fixed and the temperature of those in the second layer is controlled by the Langevin method[19] at 85 K with a Debye temperature of 240 K. The velocity Verlet method is applied for the integration of Newton's equation of motion with a time step Δt of 2 fs.

C. Calculation of pressure tensor distribution

The interfacial tensions and contact angle are derived from the two-dimensional pressure tensor distribution of the droplet. Weng *et al.*[20] calculated local pressure profiles and surface tensions of L-J liquid film system in which the calculation cell was divided into thin slabs and the one-dimensional distribution of pressure tensor was calculated by locally applying the virial theorem to each slab. In our study, extending this calculation method to the two-dimensional distribution, the calculation cell is evenly divided into small bins by intersecting planes parallel to the xy- and yz-planes, and the pressure tensor $\mathbf{P}^{ab}$ of the bin at a-th row and b-th column is calculated by using the following equation:

$$\mathbf{P}^{ab} = \frac{1}{V^{ab}} \left\langle \sum_{i \in V^{ab}} m_i \mathbf{v}_i \otimes \mathbf{v}_i + \sum_i^N \sum_{j(<i)}^N w_{ij}^{ab} \mathbf{r}_{ij} \otimes \mathbf{f}_{ij} \right\rangle. \quad (8)$$

In the right-hand side of Eq. (8), the first and second terms are the kinetic and force contributions to the bin of volume
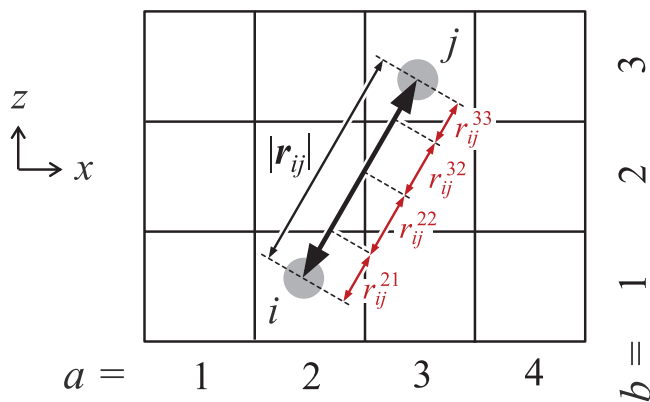
FIG. 1. Example of pressure contribution from atom pair i-j to each bin.

V^{ab}, respectively, and the brackets denote the time average of these terms. All molecules i of mass m_i and velocity $\mathbf{v}_i$ in the bin contribute the first kinetic term. The inter-molecule interactions, for which the relative position and force vectors $\mathbf{r}_{ij}$ and $\mathbf{f}_{ij}$ pass through the bin (a, b), contribute the force term. The force term contains a weighting function w_{ij}^{ab} given as the length fraction of $|\mathbf{r}_{ij}|$ in the bin. For example, the effect of interaction between the molecules i and j in bins $(a, b) = (2, 1)$ and $(3, 3)$, shown in Fig. 1, is added to the pressure tensor of bins $(2, 1)$, $(2, 2)$, $(3, 2)$, and $(3, 3)$ through the weighting function $w_{ij}^{ab} = r_{ij}^{ab}/|\mathbf{r}_{ij}|$.

For the calculation of solid-liquid interfacial tension, the force contributions of wall molecules are treated the same as those of a wall potential that has no structure,[11,17] hence the interactions between argon and wall molecules contribute to the pressure tensor component only in the normal direction to the wall. Therefore pressure tensor components P_{xx} and P_{xz} are calculated by using inter-molecular forces only between argon molecules, while inter-molecular forces between argon and wall molecules are included for the calculation of P_{zz}. The calculation cell is divided into 131×60 bins with a size of 0.189×0.2 nm^2 in xz-plane, and the pressure tensor components are calculated by averaging the simulation results over 20 ns.

III. RESULTS AND DISCUSSION

A. Density and pressure tensor distribution

Figure 2 displays snapshots and two-dimensional density distributions of a hemicylindrical droplet on a solid surface with different fluid-wall interaction coefficient η. These density distributions are calculated by averaging the position of argon molecules over 20 ns. The origins of x- and z-coordinate are set at the droplet center of the mass and the bottom edge of the system, respectively. The surface becomes more wettable and an adsorption layer is formed near the liquid-vapor interface as the value of η increases as shown in Fig. 2.
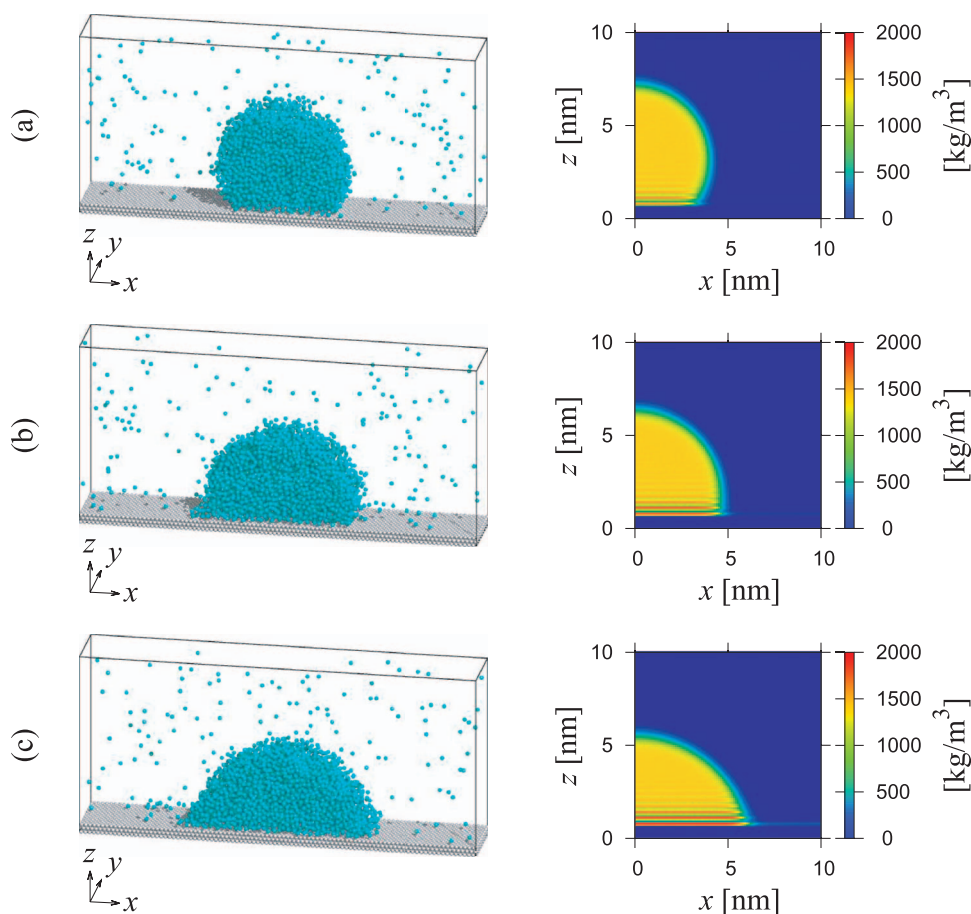

FIG. 2. (Left) Snapshots of a hemicylindrical argon droplet on a solid surface with a calculation region size of $26.0 \times 4.3 \times 12.0$ nm^3 and (right) two-dimensional density distributions of argon molecules. The fluid-wall interaction coefficients are (a) $\eta = 0.2$, (b) $\eta = 0.3$, and (c) $\eta = 0.4$.
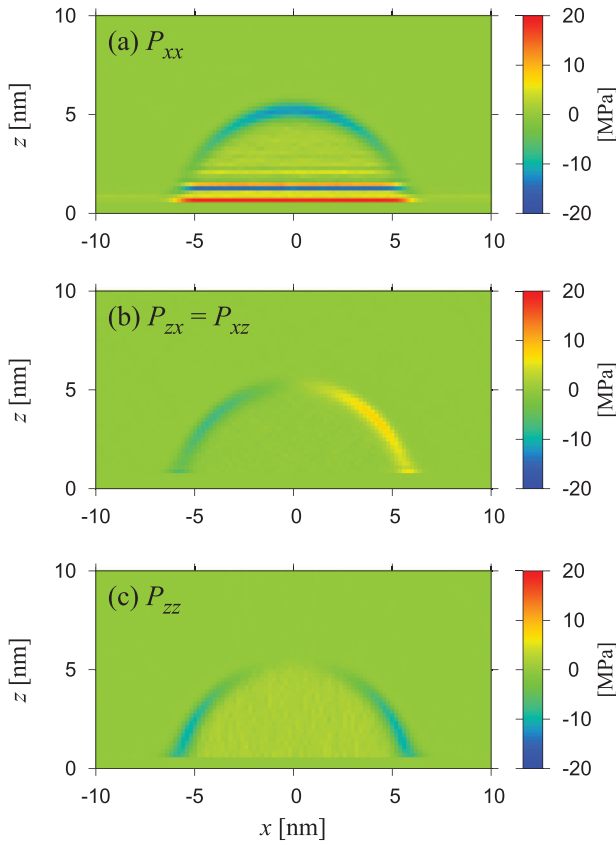
FIG. 3. Two-dimensional distributions of pressure tensor components in a Cartesian coordinate system (a) P_{xx}, (b) P_{xz}, and (c) P_{zz} for the droplet on a solid surface with a fluid-wall interaction coefficient $\eta = 0.4$. Because of pressure tensor symmetry, P_{xz} is equal to P_{zx}.

By applying Eq. (8) to a hemicylindrical droplet, the following two-dimensional pressure tensor can be obtained:

$$\mathbf{P} = \begin{pmatrix} P_{xx} & P_{xz} \\ P_{zx} & P_{zz} \end{pmatrix}. \tag{9}$$

The matrix $\mathbf{P}$ is symmetric due to the symmetric property of Eq. (8) which is in accordance with macroscopic scale stress tensor. The distributions of the components of $\mathbf{P}$ in a droplet on a solid surface with $\eta = 0.4$ are shown in Fig. 3. For these distributions, a Cartesian coordinate system identical with the one for the density distributions in Fig. 2 is adopted.

It is observed that the value of off-diagonal component P_{xz} is approximately zero at liquid and vapor bulk and changes along the liquid-vapor interface while the diagonal components P_{xx} and P_{zz} show different features.

B. Invariant distribution and transition layer

Focusing on the value of the diagonal components P_{xx} and P_{zz} in Fig. 3, both P_{xx} and P_{zz} have almost the same constant positive values in the liquid bulk region, and this is due to the Laplace pressure. However, in the vicinity of each interface, there exists a region where the distributions of P_{xx} and P_{zz} are different from those in the bulk region, and the pressure therein is anisotropic.

In order to evaluate the thickness of these regions, the trace I_1 and determinant I_2 of the pressure tensor $\mathbf{P}$ are em-

ployed as invariants that are independent of the coordinate system,

$$I_1 = P_{xx} + P_{zz}, \tag{10}$$

$$I_2 = P_{xx} P_{zz} + P_{xz}^{\,2}. \tag{11}$$

By using these invariants, mean principal pressure P_{ave} and maximum principal pressure difference ΔP_{max} are respectively defined by

$$P_{ave} = \frac{P_{xx} + P_{zz}}{2} = \frac{I_1}{2}, \tag{12}$$

$$\Delta P_{max} = \sqrt{(P_{xx} - P_{zz})^2 + 4P_{xz}^{\,2}} = \sqrt{I_1^{\,2} - 4I_2^{\,2}}. \tag{13}$$

The values of $-P_{ave}$ and ΔP_{max} correspond to mean principal stress and maximum stress difference in continuum mechanics, respectively.

Figure 4 shows the distributions of invariants P_{ave} and ΔP_{max} calculated from the components of $\mathbf{P}$ in Fig. 3. In both distributions of Fig. 4, there exist regions which henceforth are called "transition layers" where the values of P_{ave} and ΔP_{max} change abruptly in the vicinity of each interface. This is especially apparent in Fig. 4(b), where a positive value of ΔP_{max} is obtained in the transition layers under anisotropic pressure, while the value approaches zero in the bulk region under isotropic pressure. The thicknesses of liquid-vapor and solid-liquid transition layer are both estimated about 2 nm from the distribution of ΔP_{max}. In addition, the solid-vapor transition layer, which is thinner than the others, is also observed just above the solid wall with about the thickness of single bin.

Since each transition layer has a certain thickness with a specific distribution of invariants along each interface as shown in Fig. 4, there exists an overlap region among the transition layers in the vicinity of the three-phase interface. This overlap is considered to be negligible in the macroscopic
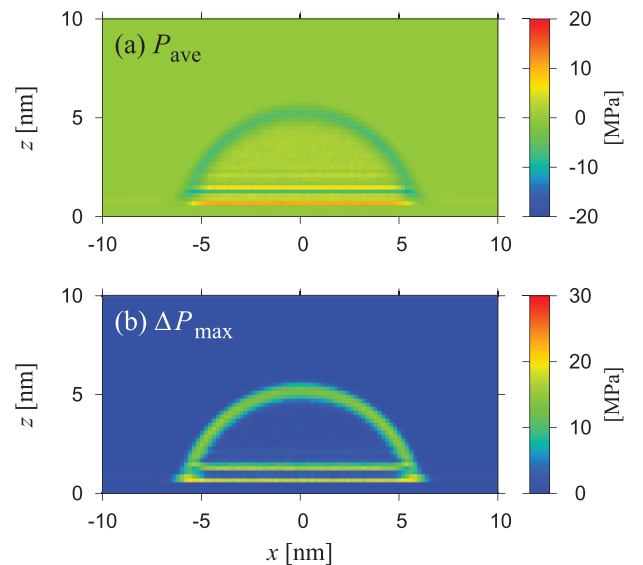

FIG. 4. Two-dimensional distributions of the (a) mean principal pressure P_{ave}, and (b) maximum principal pressure difference ΔP_{max} for the droplet on a solid surface with a fluid-wall interaction coefficient $\eta = 0.4$.
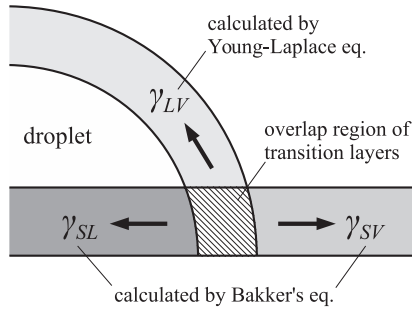
FIG. 5. Schematic of the force balance at the three-phase interface of a liquid droplet, where each interface has a transition layer with a certain thickness as indicated in Fig. 4. Three interfacial tensions are calculated from the regions where the transition layers do not overlap in the following discussion.

model of interface in Eq. (1), where the three interfacial tensions are described to act at the contact line and not inside the overlap region. The schematic of the three transition layers and the overlap region is exhibited in Fig. 5. Considering this feature, we extract the distribution of the anisotropic pressure in each two-phase transition layer, and hence use it to calculate each interfacial tension from regions without overlap among them as described in Fig. 5 and in the following discussion.

C. Measurement of contact angle

From the distributions of the invariants, each transition layer can be extracted as the change in the value of P_{ave} and ΔP_{max}. The value of P_{ave} is smaller in the liquid-vapor transition layer than those in the bulk region as seen in Fig. 4(a), and contact angle θ is approximated by fitting a least squares circle to the bins considered to be inside the liquid-vapor transition layer. In practice, the position of the center and radius of the fitting circle is obtained by using the least square method to the position of the bins with $P_{\text{ave}} < -2.5$ MPa and $z > 1.2$ nm. The contact angle is defined as the angle between this fitting circle and the wall surface, where the position of the wall surface is set to the equilibrium position of the wall molecules in the top layer. Indeed the definition of wall surface position includes arbitrariness, and it is more likely that it is positioned between the first adsorption layer and the present position, but the contact angle obtained with the present position has turned out to give a good match with the predicted contact angle described later in Sec. III F.

D. Diagonalization of pressure tensor

Besides the invariants of the pressure tensor **P**, the direction and magnitude of the principal pressure calculated from **P** are used for the investigation of the transition layers and their overlap region. The symmetric matrix **P** can be diagonalized to $\mathbf{P}_{\text{diag}}$ as

$$\mathbf{P}_{\text{diag}} = \mathbf{U}^{-1}\mathbf{P}\mathbf{U} = \begin{pmatrix} P_1 & 0 \\ 0 & P_2 \end{pmatrix}$$

$$= \begin{pmatrix} P_{\text{ave}} + \frac{\Delta P_{\text{max}}}{2} & 0 \\ 0 & P_{\text{ave}} - \frac{\Delta P_{\text{max}}}{2} \end{pmatrix}, \quad (14)$$

$$\mathbf{U} = (\,\mathbf{v}_1 \quad \mathbf{v}_2\,) = \begin{pmatrix} \cos\phi & -\sin\phi \\ \sin\phi & \cos\phi \end{pmatrix}, \quad (15)$$

$$\cos(2\phi) = \frac{P_{xx} - P_{zz}}{\Delta P_{\text{max}}}, \quad (16)$$

$$\sin(2\phi) = \frac{2P_{xz}}{\Delta P_{\text{max}}}, \quad (17)$$

where the eigenvalues P_1 and P_2, respectively, denote the principal pressures corresponding to eigenvectors $\mathbf{v}_1$ and $\mathbf{v}_2$, and the principal directions are obtained as ϕ from the eigenvectors.

The principal pressures around the overlap region for the droplet with $\eta = 0.4$ are indicated by arrows superimposed on its density distribution in Fig. 6. Here two pairs of arrows are produced at each bin in Fig. 3, while the bins used for the calculation of the density are sized by half in the length scale. An inline arrow pair toward the center denotes a compressive principal pressure with a positive eigenvalue, while a inline arrow pair outward the center denotes a tensile principal pressure with a negative eigenvalue, and the length of the arrows indicates the magnitude for both.

The direction of the arrows shown in Fig. 6 is examined below. Notable tensile principal pressure is observed around the liquid-vapor transition layer, whose direction is tangential to the liquid-vapor interface. Principal pressure tangential to the interface also exists around the solid-liquid transition layer, where the pressure has both tensile and compressive directions because of the inhomogeneous density distribution. Finally, the vectors in the liquid-vapor and solid-liquid transition layers intermix inside the overlap region, hence the principal directions there are tangential to neither the liquid-vapor nor the solid-liquid interface.

E. Three interfacial tensions

The invariants and principal pressure calculated in Subsection III D inside the overlap region are different from those in the two-phase transition layers. Because of this, the components of **P** in the regions away from the overlap region are used for the calculation of the interfacial tensions.

According to Bakker's equation,[11] interfacial tensions γ of a flat interface normal to the z-direction can be calculated from the difference of pressure tensor components as

$$\gamma = \int (P_{zz} - P_{xx})dz, \quad (18)$$

where the integration range has to cover the whole interface. This equation is used for calculation of γ_{SL} and γ_{SV}. As an example, the one-dimensional distributions of P_{xx} and P_{zz} at $x = 0$ are shown in Fig. 7, which are used to calculate γ_{SL} of the droplet on a solid surface with $\eta = 0.4$. From the distribution of P_{xx} in Fig. 7, the area between $z = 0.7$ nm and $z = 3.0$ nm is considered to contain the solid-liquid transition layer, and is employed as the integration range of Eq. (18). In practice, for the case of $\eta = 0.4$, the mean value of $(P_{xx} - P_{zz})$ in the region of $|x| \leq 2.0$ nm away from the overlap,
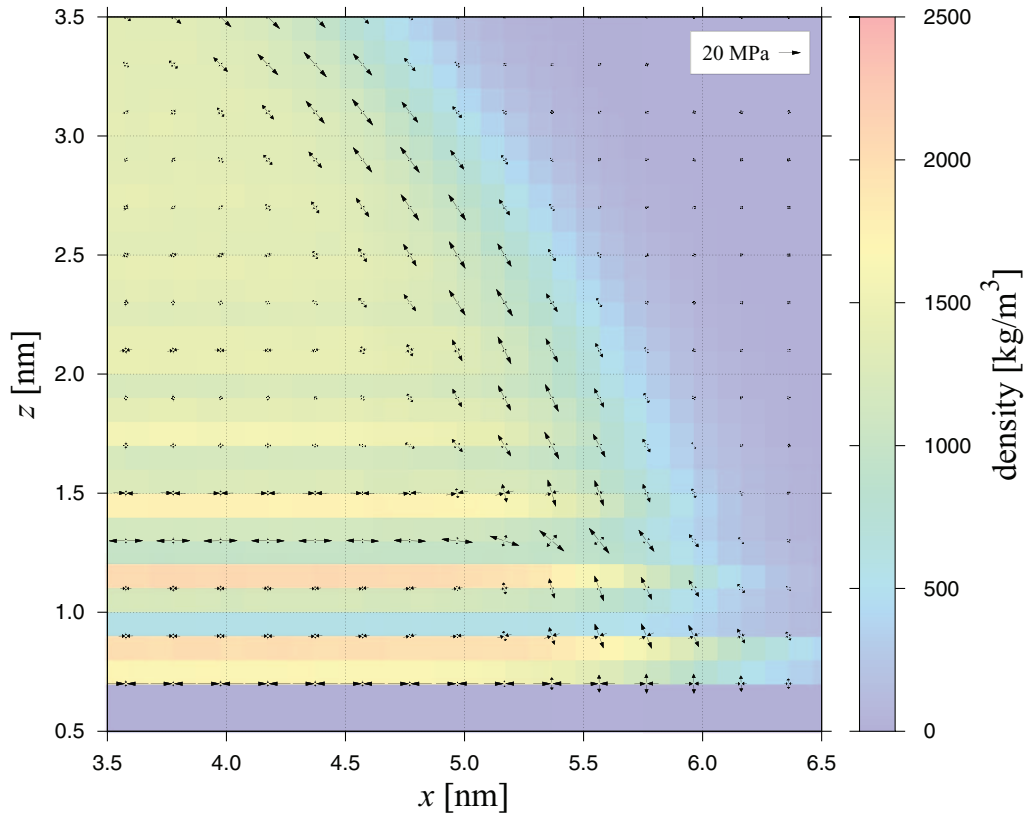
FIG. 6. Principal pressures inside and around the overlap region for the droplet on a solid surface with $\eta = 0.4$ superimposed on its density distribution. Two inline arrow pairs are produced at every bin of Fig. 3 with a size of 0.189×0.2 nm^2 in xz-plane, while the size of the bin used for the density distribution is 0.094×0.1 nm^2. The direction and length of the arrows, respectively, correspond to the direction and magnitude of the principal pressure of **P**, where inline arrow pairs toward and outward the center indicate the compressive and tensile principal pressures, respectively.

where the distributions are similar to those at $x = 0$, is integrated along the z-direction, and the same range between $z = 0.7$ nm and $z = 3.0$ nm is used for integrating the mean value of $(P_{xx} - P_{zz})$ at $|x| \geq 7.0$ nm to obtain γ_{SV}. Different ranges are used for the calculation of γ_{SL} and γ_{SV} for the cases with
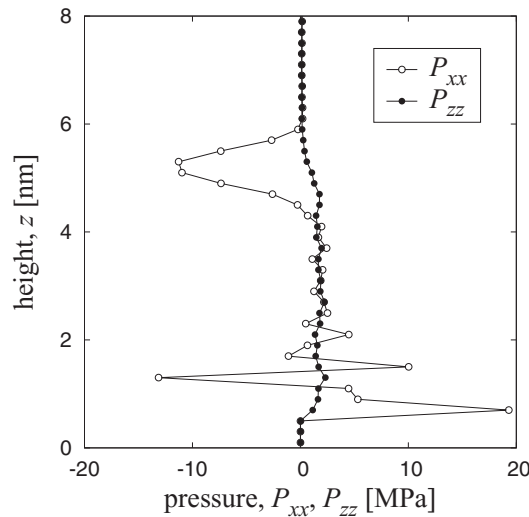

FIG. 7. One-dimensional distributions of P_{xx} and P_{zz} at the center plane of $x = 0$ nm for the droplet on a solid surface with $\eta = 0.4$. The positive isotropic pressure inside the liquid bulk is due to the Laplace pressure.

different η to exclude the overlap. We have indeed calculated the distribution of the pressure tensor around the solid-liquid interface in a quasi-one-dimensional flat system for liquid argon as well as that for water-alcohol mixture,[17] and the basic feature was the same as in Fig. 7 except for the fact that the isotropic pressure inside the liquid bulk was the same as those in vapor and solid bulk because the flat interface does not produce Laplace pressure. It should also be noted that the values of γ_{SL} and γ_{SV} obtained by using Eq. (18) are not absolute but "relative" to those of a solid-vacuum interface, and this is discussed later in this subsection.

Different from the interfacial tensions γ_{SL} and γ_{SV}, γ_{LV} should not be calculated by using Eq. (18) because the liquid-vapor interface is hemicylindrical. In order to calculate γ_{LV}, the Young-Laplace equation

$$\frac{\gamma_{LV}}{R} = P_L - P_V \tag{19}$$

is used instead, where R, P_L, and P_V denote the radius of the droplet and the pressures at liquid and vapor bulk, respectively. Here the radius R is obtained from the fitted circle mentioned in the Subsection III C, while P_L and P_V are evaluated as the spatial averages of P_{ave} in liquid and vapor bulk shown in Fig. 4(a), respectively.

Figure 8 displays the relation between η and the interfacial tensions evaluated by using Eqs. (18) and (19). Note that the values γ_{SV} and γ_{SL} are not absolute but relative ones as
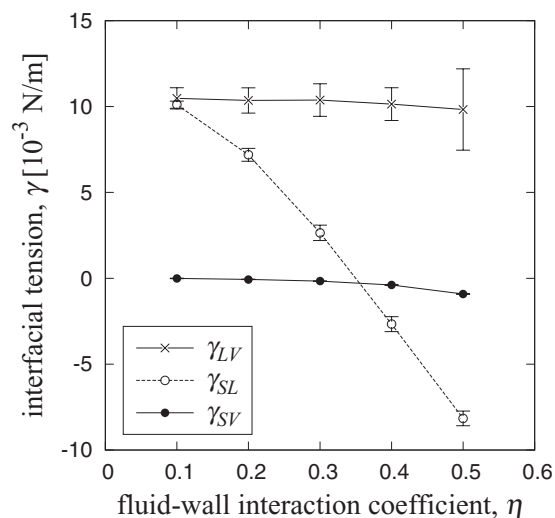
FIG. 8. Relation between fluid-wall interaction coefficient η and interfacial tensions in the droplet system. Bakker's equation[11] is employed to calculate the relative interfacial tensions of γ_{SL} and γ_{SV}, while γ_{LV} is the absolute value and calculated via the Young-Laplace equation.

FIG. 9. Relation between fluid-wall interaction coefficient η and cosine of contact angle θ of the droplet. Measured contact angles and ones derived from Young's equation using the interfacial tensions in Fig. 8 are displayed.

described later in this section, and therefore negative interfacial tensions are not unphysical. The value of γ_{SV} is almost zero and slightly decreases to become negative with a larger η. Similarly, γ_{LV} is almost constant regardless of η because the liquid-vapor interface is not affected by the solid surface. The error-bar is relatively large for larger η values because the bulk region is small due to the small contact angle in our case. A similar value of $\gamma_{LV} = 11.9 \times 10^{-3}$ N/m in MD simulation is reported by Yaguchi *et al.*[21] On the other hand, although the value of γ_{SL} is close to γ_{LV} at $\eta = 0.1$, it becomes smaller and eventually negative with the increase of η. The change in the value of γ_{SL} is the main cause of increase in droplet wettability.

The meaning of the "relative" solid-liquid and solid-vapor interfacial tensions, which take negative values, should be addressed here. Because in this study the interaction between solid particles is modeled by the harmonic potential in which the interaction pairs are prescribed to connect the nearest neighbors and zero point of the potential energy is set at an equilibrium distance, the total potential energy of a crystal solid surface without thermal vibrations placed in vacuum is zero and solid bulk has no energetic advantage over surface in this model even though the particles in solid bulk have more interaction pairs than those at the surface. When a small amount of argon molecules is adsorbed onto this solid surface, the total potential energy becomes negative because the L-J potential for the fluid-wall interaction has a negative well. This means that the values of γ_{SL} and γ_{SV} calculated by using Eq. (18) are relative to vacuum and become apparently negative due to the zero-point setting of the harmonic potential model. Since only the difference between the solid-liquid and solid-vapor interfacial tensions has influence on wettability as shown in Eq. (1), relative values are enough for the two for the evaluation in Sec. III F. On the other hand, the values of γ_{LV} calculated by using Eq. (19) are absolute ones and always positive.
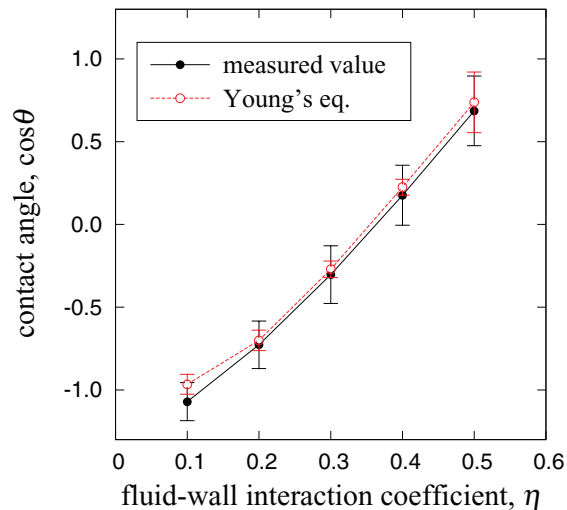
F. Interfacial tension balance and contact angle

The relation between η and cosine of the measured contact angle θ is shown by black circle symbols in Fig. 9. The two seem to be linearly correlated, as also reported by Maruyama *et al.*[22] The white circle symbols in Fig. 9 display the η-$\cos\theta$ relation in which $\cos\theta$ values are obtained by substituting the interfacial tension values in Fig. 8 into Young's equation in Eq. (1). They correspond well to the measured contact angle, and this shows that the relation between the balance among evaluated interfacial tensions and measured contact angle is consistent with Young's equation. The $\cos\theta$-η relation agrees well with the earlier reports[14, 15] which show slight deviation from first-order correlation. In addition, Ingebrigtsen and Toxvaerd[12] reported the deviation of contact angle values from those obtained by Young's equation using interfacial tensions for larger η values, and they claimed that this was due to the weak short-ranged L-J dispersion force-field. This deviation is also shown in the results of Leroy and Müller-Plathe.[14] In our case the contact angle values include larger error for large η values, and it is difficult to evaluate the feature.

IV. CONCLUDING REMARKS

MD simulations of single hemicylindrical argon droplet on a solid surface were performed. By applying the virial theorem to the droplet, two-dimensional distributions of the pressure tensor and its invariants were calculated. The change in the distributions of these invariants indicated two-phase transition layers of a certain thickness in which the pressure is anisotropic, and the contact angle was measured by using least square fitting circles. The distribution of the principal pressure, which is derived by diagonalizing the pressure tensor, revealed a specific feature of intermix inside the overlap region of the two-phase transition layers. Three interfacial tensions were derived in the region away from this overlap area and showed that the relation between contact angle

and balance among three interfacial tensions turned out to correspond well to Young's equation in our simulation system, indicating that Young's equation holds in nanoscale.

ACKNOWLEDGMENTS

[1] P. G. de Gennes, F. Brochard, and D. Quéré, *Capillarity and Wetting Phenomena: Drops, Bubbles, Pearls, Waves* (Springer, 2004).
[2] T. Young, Philos. Trans. R. Soc. London **95**, 65 (1805).
[3] L. R. White, J. Chem. Soc. Faraday Trans. 1 **73**, 390 (1977).
[4] L. Boruvka and A. W. Neumann, J. Chem. Phys. **66**, 5464 (1977).
[5] A. Marmur, J. Colloid Interface Sci. **186**, 462 (1997).
[6] M. N. Popescu, G. Oshanin, S. Dietrich, and A. M. Cazabat, J. Phys.: Condens. Matter **24**, 243102 (2012).
[7] V. K. Kumikov and K. B. Khokonov, J. Appl. Phys. **54**, 1346 (1983).
[8] W. R. Tyson and W. A. Miller, Surf. Sci. **62**, 267 (1977).
[9] T. D. Blake, A. Clarke, J. D. Coninck, and M. J. de Ruijter, Langmuir **13**, 2164 (1997).
[10] T. Werder, J. H. Walther, R. L. Jaffe, T. Halicioglu, and P. Koumoutsakos, J. Phys. Chem. B **107**, 1345 (2003).
[11] M. J. P. Nijmeijer, C. Bruin, A. F. Bakker, and J. M. J. van Leeuwen, Phys. Rev. A **42**, 6052 (1990).
[12] T. Ingebrigtsen and S. Toxvaerd, J. Phys. Chem. C **111**, 8518 (2007).
[13] J. H. Weijs, A. Marchand, B. Andreotti, D. Lohse, and J. H. Snoeijer, Phys. Fluids **23**, 022001 (2011).
[14] F. Leroy and F. Müller-Plathe, J. Chem. Phys. **133**, 044110 (2010).
[15] E. M. Grzelak and J. R. Errington, J. Chem. Phys. **128**, 014710 (2008).
[16] D. Seveno, T. D. Blake, and J. D. Coninck, Phys. Rev. Lett. **111**, 096101 (2013).
[17] D. Surblys, Y. Yamaguchi, K. Kuroda, M. Kagawa, T. Nakajima, and H. Fujimura, J. Chem. Phys. **140**, 034505 (2014).
[18] J. Z. Tang and J. G. Harris, J. Chem. Phys. **103**, 8201 (1995).
[19] J. Blömer and A. E. Beylich, Surf. Sci. **423**, 127 (1999).
[20] J. G. Weng, S. Park, J. R. Lukes, and C. L. Tien, J. Chem. Phys. **113**, 5917 (2000).
[21] H. Yaguchi, T. Yano, and S. Fujikawa, J. Fluid Sci. Technol. **5**, 180 (2010).
[22] S. Maruyama, T. Kuruashige, S. Matsumoto, Y. Yamaguchi, and T. Kimura, Microscale Thermophys. Eng. **2**, 49 (1998).